

REGISTERED

*RU267*

*#5155*

*GE-AK82*

Distribution of Flice Sizes in the Eastern Beaufort Sea Shear Zone

*2576*

by

William J. Stringer

Assisted by

Joanne E. Groves

Richard D. Handler

Coert Ousted

Geophysical Institute

University of Alaska

Fairbanks, Alaska

October 8, 1982

NCAA-008 Contract No. 81-3AC06147

*Amstat 2*

LIBRARY REFERENCE VOLUME  
ENVIRONMENTAL STUDIES BRANCH  
MINERALS MANAGEMENT SERVICE  
DEPARTMENT OF THE INTERIOR  
WASHINGTON, D.C.

Distribution of Floe Sizes in the Eastern Beaufort Sea Shear Zone

by

William J. Stringer

Assisted by

Joanne E. Groves

Richard D. Henzler

Coert Olmsted

Geophysical Institute

University of Alaska

Fairbanks, Alaska

October 8, 1982

NOAA-OCS Contract No. 81-RAC00147

## Distribution of Floe Sizes in the Eastern Beaufort Sea Shear Zone

### Introduction

The shear zone is a region of dynamic ice behavior resulting from interaction between the static shorefast ice zone and the pack ice **in** the **Beaufort gyre**. The distribution of floe sizes within the shear zone is of interest to the Outer Continental **Shelf** Environmental Assessment Program in relation to the behavior of spilled oil. First, there is the problem of spilled oil in a region of broken ice where the number and size of floes is important when considering the spread of spilled oil. Second, there is the problem of the rate of introduction of **oil** which had been incorporated into the ice, into the oceanic waters. Here, the total floe perimeter exposed to the water at any time is an important factor.

The results and processes described in this paper depend on a clear understanding of the shear zone and the events **which** occur in that region. Crowder, et al., 1973 describe the general process creating the shear zone: "The pack ice as a whole is rotating clockwise and slipping within a narrow region (~50km) at the boundary" between the seasonal pack ice and **the shorefast** ice. Kovacs and Mellor (1974) call this region the "shear zone" and describe the region and related processes further:

"The ice in the shear zone is subjected to the highest stresses. These occur when the pack ice is driven toward the coast. Unable to overcome the resistance of the more monolithic fast ice, the drift of the irregular floes within the shear zone is arrested and the floes are gradually pushed tighter as more of the outer pack ice comes into play. The stresses developed as these **floes** impinge

upon each **other** or push against weaker ice that has formed in refrozen leads are often sufficient **to** cause the failure or crushing of one of the participating ice sheets. The result (spatially) is a haphazard accumulation of ice blocks of a most irregular and formidable appearance. When high normal and tangential forces are **at** play between the fast ice and the moving pack ice, extensive shearing and grinding of the ice occur. The **result** is a ground-up consolidated mass of ice called a shear ridge. These ridges, common along the Alaskan coast, are often tens **of** kilometers in length and frequently 4 m high. At times the shearing stresses are so intense that a sequence of shear ridges develops into a **hummock** field so formidable that no icebreaker in existence or under construction can penetrate it."

While the shear zone is a very useful concept that is quite valid as a long-term description of the interaction between fast ice and pack ice in the Beaufort **Gyre**, instantaneous ice behavior in the offshore region is not always adequately described by the shear zone concept. Consequently, some caution must be exercised in basing decisions and plans concerning development of offshore areas on the mental picture this concept conjures.

Certainly on a long-term average, the Beaufort Sea ice pack is rotating largely as a whole with a rather narrow (50-100 km) peripheral zone where the transition between static shorefast ice and the transiting pack takes place. Observations based on Landsat imagery show that on many specific occasions, there is a pronounced edge of shorefast ice and just beyond, fractured pack ice moving along this edge (usually **toward** the west in the **Beaufort** Sea). Often after such episodes considerable

shear ridge-building activity can be seen to have taken place along the very edge of **the** shorefast ice, and the pack ice fragmentation is greatest **there**, decreasing with distance toward the Arctic pack.

However, on many occasions such slippage between shorefast and pack ice, if **it** is taking place at **all**, is occurring far seaward (over 100 km) of the normal edge of the shorefast ice. Observations by Stringer (1974), **using Landsat** imagery have shown that at times the shorefast ice extends far seaward, well past the normal shear zone during midwinter for periods up to 6 weeks in length. Furthermore, from one occasion to the next, the location of this slippage can change drastically. The well known track of the ice island, T-3, traveling with the arctic pack shows that the rotation of the pack ice is stepwise and not continuous. Hence, the shear zone is not a continuous process, but rather a series of stochastic events taking place at various distances from shore.

This paper is concerned with the distribution of the sizes of floes **created** during these events and continuing into the summer season. From the description of shear zone processes given above, one might expect that at the beginning of a slippage event that the floe sizes would tend to be rather **large** and decline with **time**. Then, after slippage ceases, if the temperature is sufficiently low, the floes would freeze together again. Several fragmentation/freezing cycles might be expected during each winter season. However, after freezing temperatures cease, the fragmentation process naturally continues into the summer. As will be shown, the fragmentation process is highly irregular during its early stages and only becomes systematic after it has progressed over a considerable period of time. It was found that in order to identify any systematic floe-division process occurring during the early stages, it was necessary **to look at** the floe size distribution occurring at much later times.

## Analysis

Clearly, if the shear zone **floe** size distribution behaves as just described, it will change with time depending on the rate with which stresses are being applied on the floes and their strength. This, in turn, will depend on the confining forces and shearing forces within the pack, and the strength history of the ice and perhaps several other factors. In order to study this process in detail, nearly continuous monitoring by an imaging satellite would be required. This is not presently possible. The number of Landsat platforms is such that observations are limited under the very best circumstances to three consecutive days out of every nine. Further limitations are imposed by cloudiness and occasional equipment failure.

However, in order to obtain even some idea of the distribution of floe sizes in the shear zone a number of Landsat scenes from the eastern Beaufort Sea were selected and enlarged for analysis purposes. Even before numerical analysis was performed, it was obvious that within the shear zone on each image many domains with differing floe size distribution could be found (see figure 1). This suggested that the process involved was much more random than had been anticipated. Because of this it was determined to limit the number of cases analyzed and spend some of the time saved on an attempt at a computer simulation of the shear zone floe generation process.

Images from four dates were chosen for analysis. On two of these, a single sample was obtained while on two others two samples were obtained. These results will be described in chronological order.

## EARLY JUNE

Example used is scene 2497-20421 obtained June 2, 1976 (see figure 1). As can be seen from examination of this image, it would appear that a wide range of floe size distributions could be obtained, depending on the location of the sample. However, this observation may be misleading. Although the frequency of the larger floe sizes may vary from area to area, the shape of the floe size distribution may be the same. It can also be seen that, as might be anticipated, floes tend to be smaller at the shoreward edge of the shear zone and become larger as one progresses into the ice pack.

In order to obtain some idea of the floe size distribution in the shear zone on this image, two more-or-less representative areas were chosen, one of 400 sq km and the other of 100 Sq km.

In the larger area 354 floes were counted of which 303 were above the threshold for measurement ( $.03 \text{ km}^2$ ). The average floe size was  $1.0 \text{ km}^2$  while the largest floe had an area of  $32 \text{ km}^2$ .

Within the smaller area 52 floes were counted of which 46 were above the threshold for measurement. The average floe size was  $1.5 \text{ km}^2$  while the largest individual floe had an area of  $18 \text{ km}^2$ .

The resulting floe size distributions are plotted in log-log format in figures 2 and 3. In figure 2 a visual best fit has been superimposed on the data for the 400 km square area. The solid line represents the relationship:  $N = 6KS^{-1.5}$  where N is the number of floes per floe size unit, S is the floe size of that unit and K is a unit constant with dimensions number per unit size.

In figure 3 a best fit similar to that in figure 2 has been plotted. This line is satisfied by the power law:  $N = 1.4 K S^{-1.3}$ .

In these power law formulations, the exponent of S describes the general relationship between number and size. The coefficients 6 and 1.4 are the number of floes of unit dimension (in this case 1 km<sup>2</sup>) in the area studied. Since the study areas differ by a factor of 4, one **would expect** these coefficients to differ by a factor of 4 for the same **floe** size distribution. Hence, normalizing to a study area of 100 km<sup>2</sup> gives  $N = 1.5 K S^{-1*5}$  for the floe size **distribution** in the larger area.



Figure 1. Land sat scene 2497-20421 obtained June 2, 1976. Rectangles outline areas used to obtain floe size distributions for this date. Larger area is  $400 \text{ km}^2$ , smaller area  $100 \text{ km}^2$ .

FLOE AREA  
vs.  
NUMBER

FIG. 2

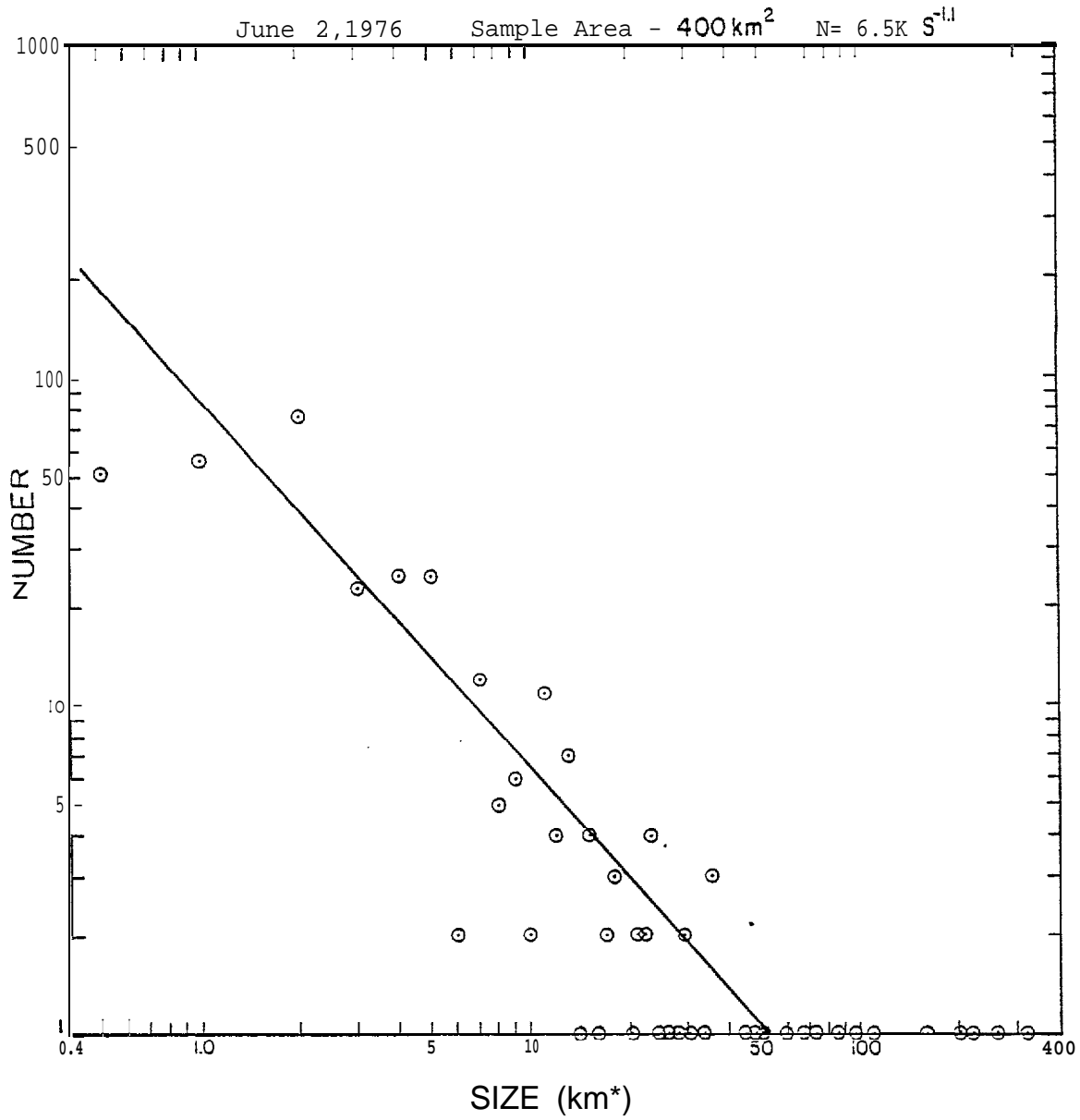


Figure 2. Log-Log plot and best visual fit of floe size versus number for 400 km<sup>2</sup> area of figure 1.

FLOE AREA  
vs.  
NUMBER

FIG. 3

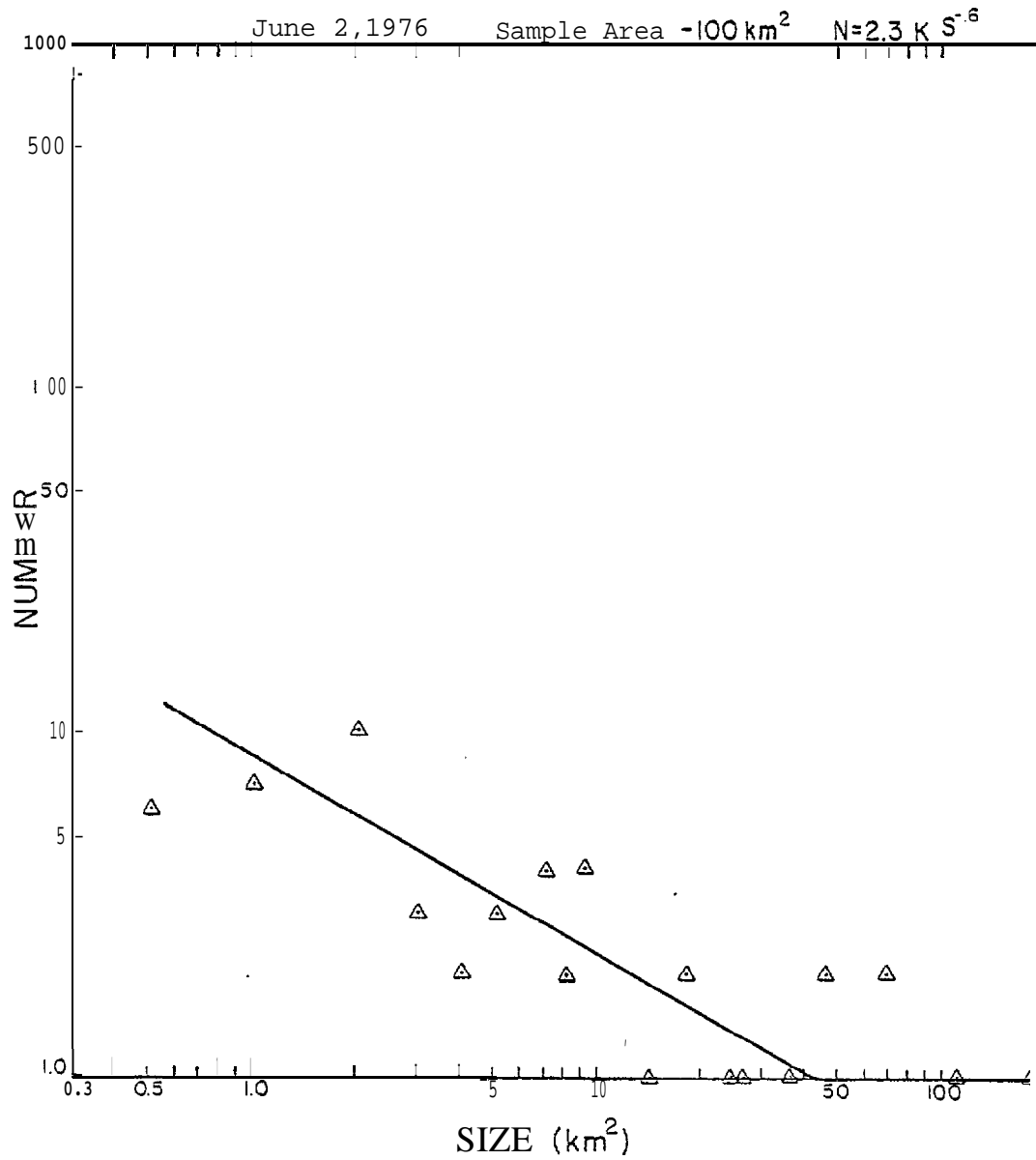


Figure 3. Log-Log plot and best visual fit of floe size versus number for 100 km<sup>2</sup> area of figure 2.

MID-JULY

The first sample used is scene 21993-20583 obtained July 7, 1980. In this case over much of the region, the ice within the shear zone has remained compact as a result of confining forces. It would be very difficult to measure individual floes within this area. However, the floes located in the open water portion of the scene appear to be essentially the same as the compacted floes except that, being surrounded by water, they can be measured. Within the 400 km<sup>2</sup> area shown 207 floes were counted of which 108 were above the threshold for measurement. The average floe size was 1.3 km<sup>2</sup> and the largest floe within the area was 53 km<sup>2</sup>.

The resulting floe size distribution has been plotted as figure 4. A power law relationship given by  $N = 4.1 KS^{-1}$  has been found to satisfy these data. Normalizing to a 100 km<sup>2</sup> area yields  $N = 1.0 KS^{-1}$ .

The second sample used is scene 1719-21031 obtained July 12, 1974. Again, as in the other July image used, ice conditions are rather compact. However, a 100 km<sup>2</sup> region with reasonably distinct floes was found. Within this region 73 floes were counted of which 62 were measured. The average floe size was 1 km<sup>2</sup> and the largest floe was 13 km<sup>2</sup>. The size distribution derived from this data set is shown as figure 5. It can be generalized by the expression  $N = 2.5 KS^{-.7}$ .

FLOE AREA  
vs.  
NUMBER

FIG. 4

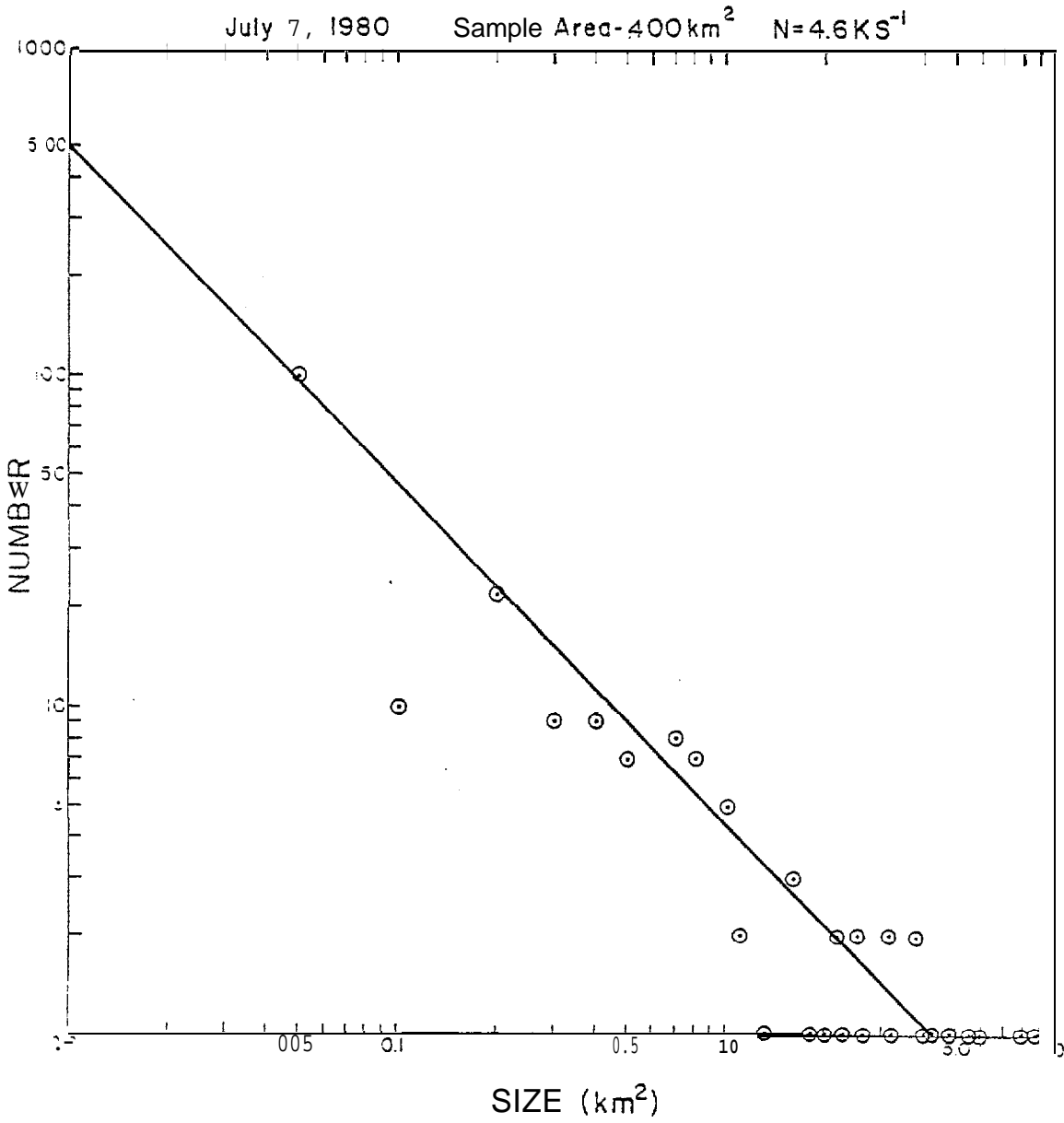


Figure 4. Log-Log plot and best visual fit of floe size versus number for 400 km<sup>2</sup> area taken from Landsat scene 21993-20583 obtained July 7, 1980.

FLOE AREA  
VS.  
NUMBER

FIG.5

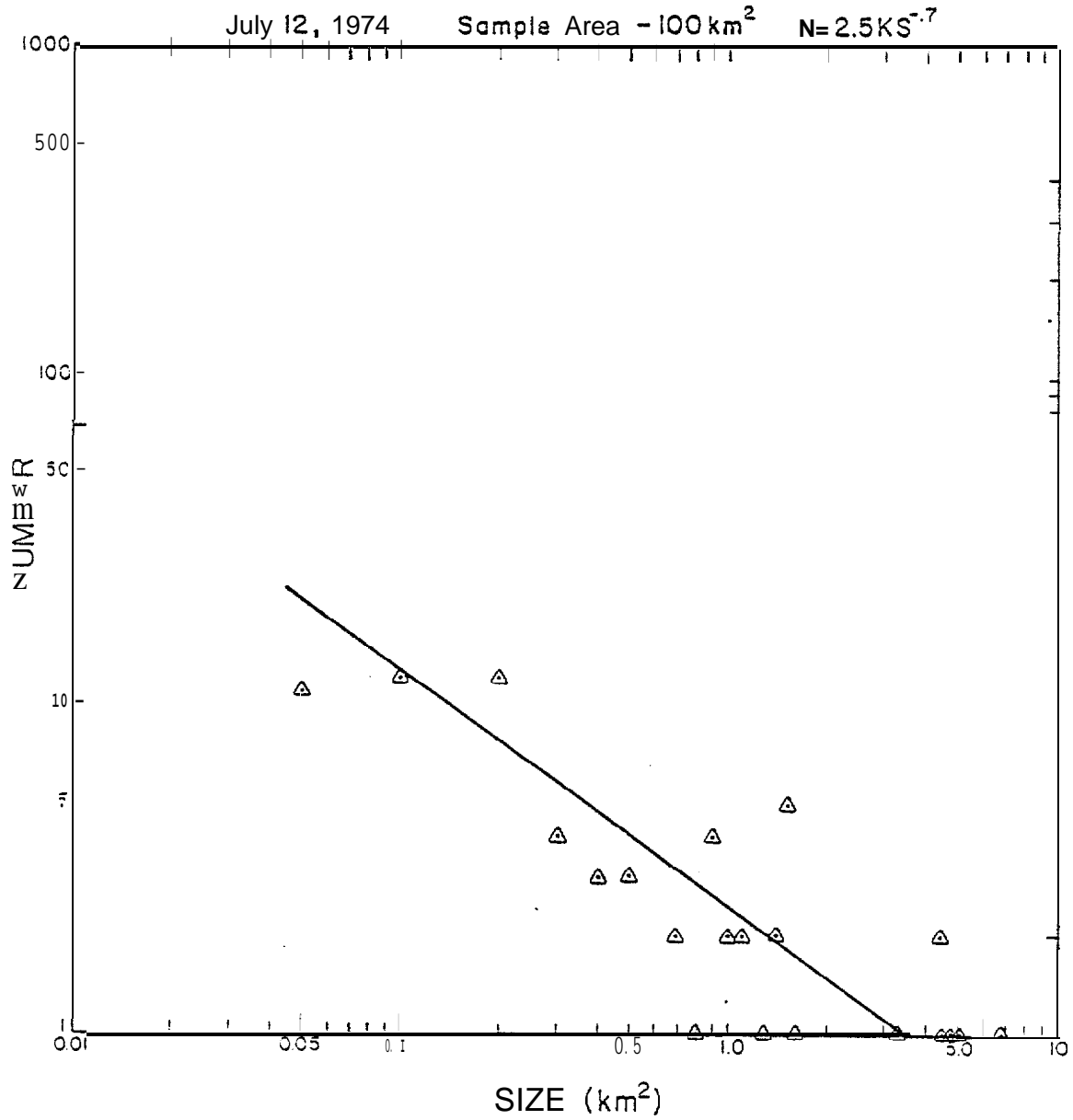


Figure 5. Log-Log plot and best visual fit of floe size versus number for 100 km<sup>2</sup> area taken from Landsat scene 1719-21031 obtained July 12, 1974.

EARLY AUGUST

The samples used were obtained from scene 22387-20440 obtained August 5, 1981 (figure 6). It is immediately obvious that the floes on this late summer scene are, in general, smaller than those on the previous examples. One might expect this as a result of the advance of season.

Two areas were selected for analysis. The first area consisted of 400 km<sup>2</sup> and contained 518 floes of which 114 were above the size threshold for measurement. The average size was 0.08 km<sup>2</sup> and the largest floe was 4.6 km<sup>2</sup>.

The second area consisted of 100 km<sup>2</sup> and contained 263 identifiable floes of which 69 were measured. The average size was .07 km<sup>2</sup> and the maximum size was 1.7 km<sup>2</sup>.

Figures 7 and 8 show the size vs. frequency distribution of floes within these areas. These distributions are idealized by the expressions:

$$N = 2 KS^{-1.8} \text{ (for figure 7) which becomes } .5 KS^{-1.8} \text{ after} \\ \text{normalization to a } 100 \text{ km}^2 \text{ area.}$$

and

$$N = .7 KS^{-1.9} \text{ (for figure 8).}$$



Figure 6. Landsat scene 22387-20440 obtained August 5, 1981. Rectangles outline areas used to obtain floe size distributions for this date. Larger area is 400 km<sup>2</sup>, smaller area 100 km<sup>2</sup>.

FLOE AREA  
vs.  
NUMBER

FIG. 7

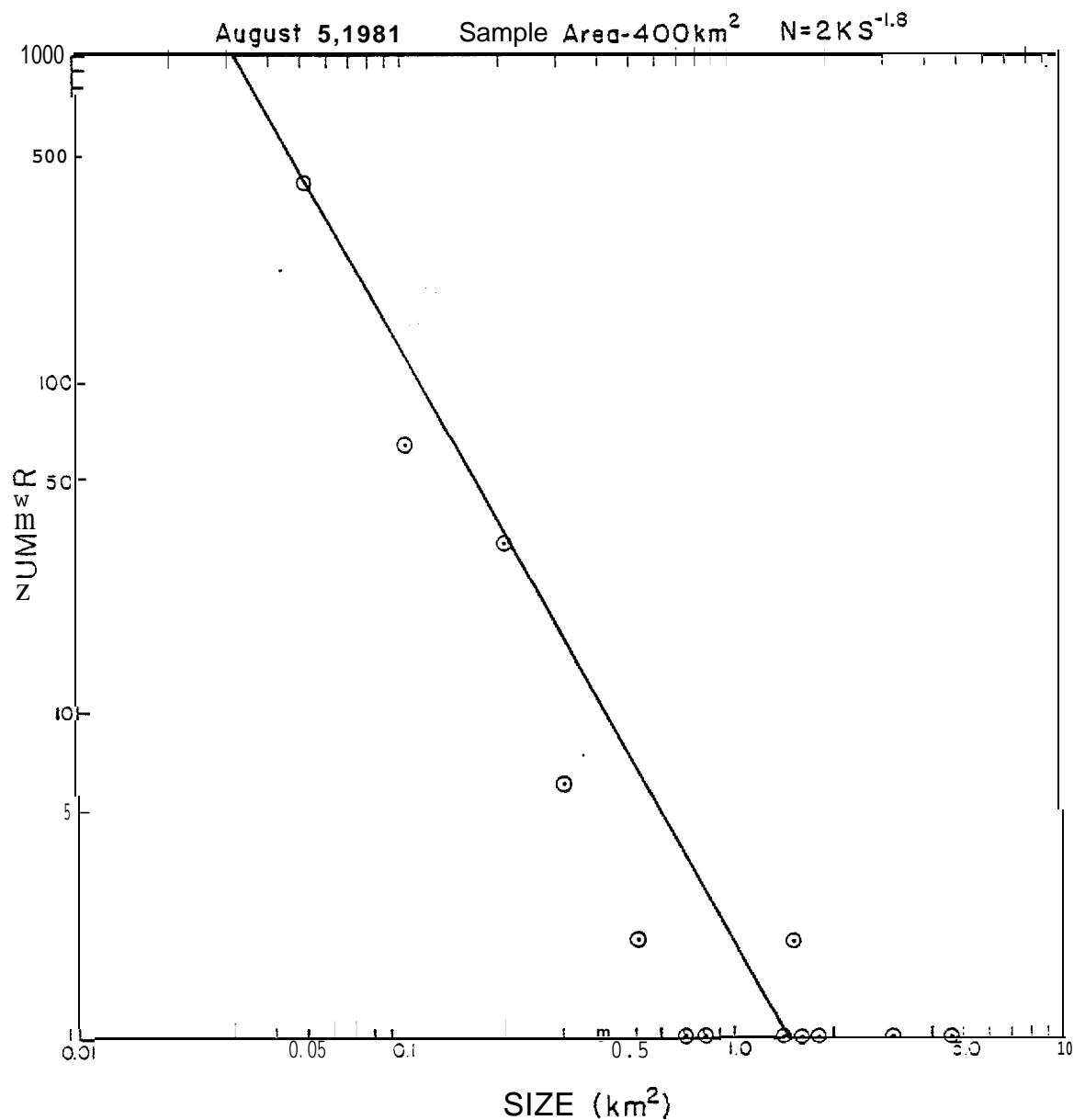


Figure 7. Log-Log plot and best visual fit of floe size versus number for 400 km<sup>2</sup> area of figure 6.

FLOE AREA  
vs.  
NUMBER

FIG. 8

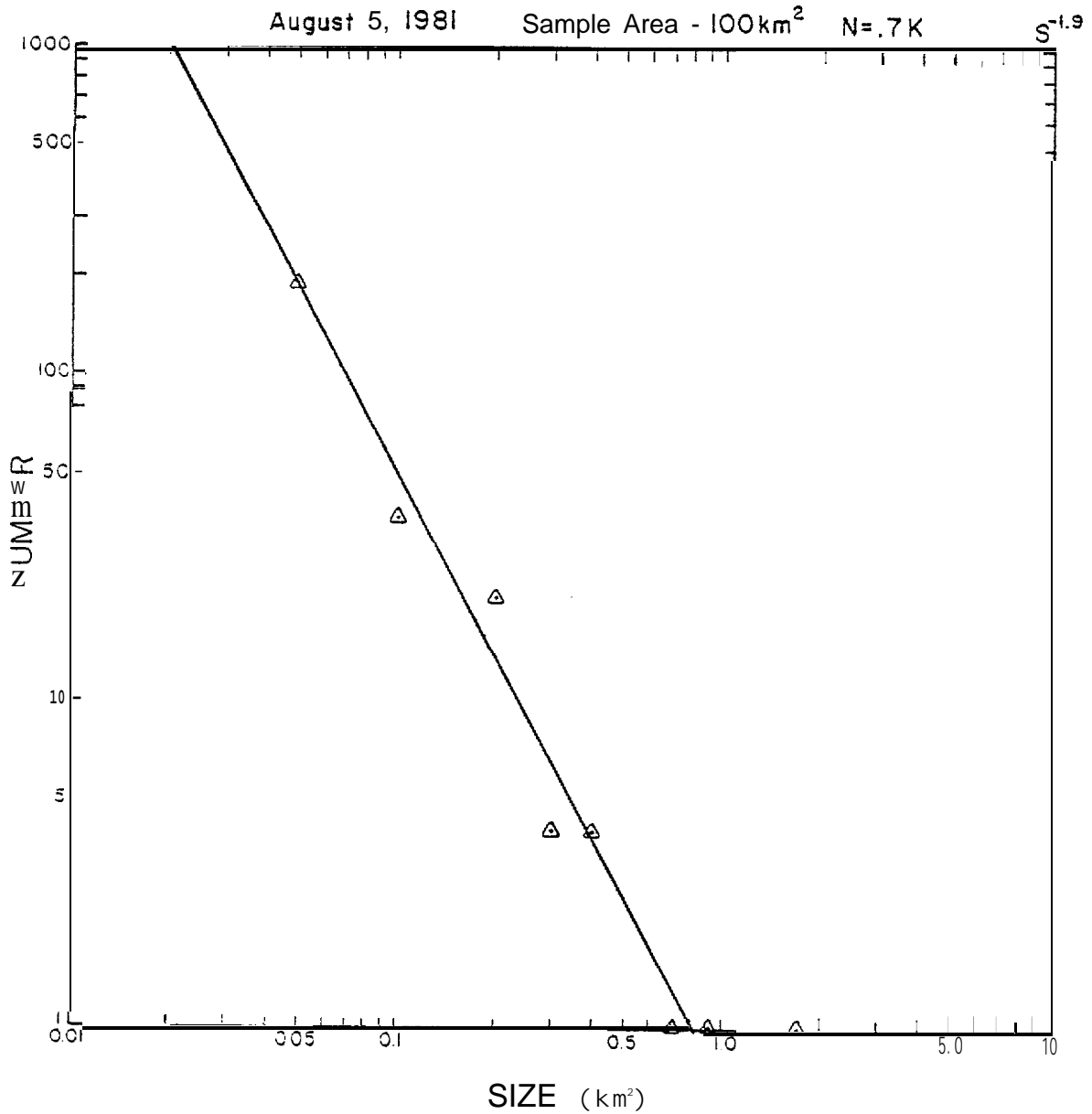


Figure 8. Log-Log plot and best visual fit of floe size versus number for 100 km<sup>2</sup> area of figure 6.

## Computer Simulation

Examination of the scatter of points comprising these measured spectra suggested a great deal of randomness. Furthermore, it appeared that the floe size distribution might change considerably from one area to the next within the same Landsat scene. (This will be discussed later.) This led to speculation about the nature of the processes creating floe size distributions. After some consideration, it was decided to attempt to develop a floe-splitting algorithm based on a principal involving a degree of randomness and compare the results of that algorithm with the measured spectra.

In determining even a simple floe-splitting algorithm, some basic assumptions must be made concerning factors related to the life-span and splitting of an ice floe. One of these assumptions is the probability of splitting taking place per unit of time. In other studies, ice floe displacements have been measured by following specific ice floes from one day to the next on Landsat imagery. From this work we know that all floes do not split on a time scale of less than one day. However, the accurate determination of the half-life of floes would be difficult and would obviously depend on conditions such as compactness of the ice pack, sea state, stress within the ice pack, etc., and therefore, would very likely change from one example to the next.

Rather than attempt to measure this quantity, the algorithm was defined in such a way that within one characteristic time,  $t$ , a given fraction of the floes would split. Since the floe size spectrum generated was quite sensitive to  $t$ , it was hoped that a value of  $t$  would become apparent by comparing synthetic spectra to the measured spectra. In this case, the fraction which undergoes splitting each characteristic time was taken as 0.5.

The next **factor** to consider is the size ratio spectrum of daughter floes derived **from the** parent floe. Although a measurement of this function might be possible, it was considered to be beyond the scope of this study, given the resources available. It was estimated that the daughter ratio was probably a **broad** distribution peaking at a 50/50 split (ratio = 1). One such distribution is provided by the ratios obtained by randomly picking numbers between 1 and 100 and using the ratio of that number and its difference from 100. (Picking 4 provides **the** ratio 1/24,) **The** resulting distribution of ratios is broadly peaked toward **ratios** in the vicinity of 1. For instance, half the ratios have a value greater than  $25/75 = 1/3$ . The smallest ratio is 1/50.

In performing the algorithm, a single floe with size  $10^8$  **arbitrary** units was used to initiate the splitting sequence. A random number generator chose a number between 1 and 100. If the number was odd, the floe divided according to the ratio generated as described above. If the number was even, **the** floe remained undivided. Thus, the random selection of **both** the division/no division decision and the division ratio was provided by the generation of a single random number. This division procedure was then applied to **the** daughter floes (or the undivided floe) again, and then repeatedly until a specified number of divisions had been performed.

The results were somewhat surprising. Despite the apparent regularity of **the** algorithm, **the** size spectra were quite "noisy" even after as many as 15 divisions. Figure 9 is a log-log plot containing two of these spectra chosen **at** random. In order to observe the amount of irregularity in floe size distribution created by this algorithm, it was run for 25 divisions ten times and the results were averaged. Standard deviations

were found for each size category. Even the average was "noisy": there was not a smooth rate of change in the number of floes from one size range to the next. The total number of floes generated by individual runs ranged from  $6 \times 10^3$  to  $20 \times 10^3$ . In terms of the average spectra statistics, the standard deviation of number of floes in each size category was as high as 10% of the average value of that category.

Finally, it was determined to generate average curves for 4, 6, 8, 10, 13, 15, 20, 25, 30, and 35 divisions by performing each case 100 times and averaging. The family of curves shown in figure 10 is the result of these computations. The average curve for 15 divisions has been plotted on figure 9 in order to demonstrate the variation between the two single spectra and the average over 100 cases.

FLOE AREA  
VS.  
NUMBER

- ⊙ One 15 division cycle
- △ Another 15 division cycle
- ▣ 100 averaged 15 division cycles

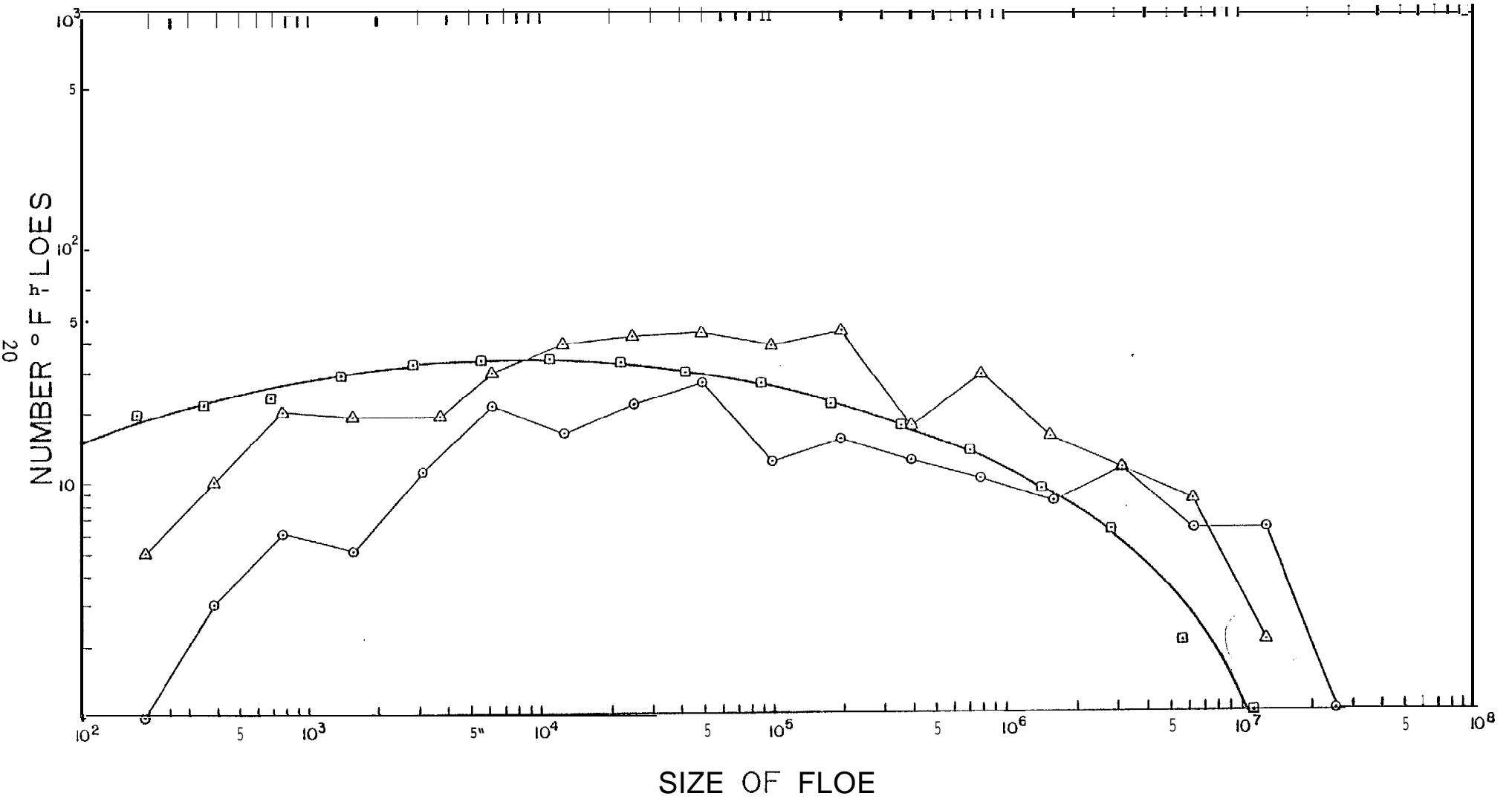


Figure 9. Log-Log plot comparing two typical results of performing floe-splitting algorithm for 15 division processes, and smooth curve obtained by averaging 100 such spectra.

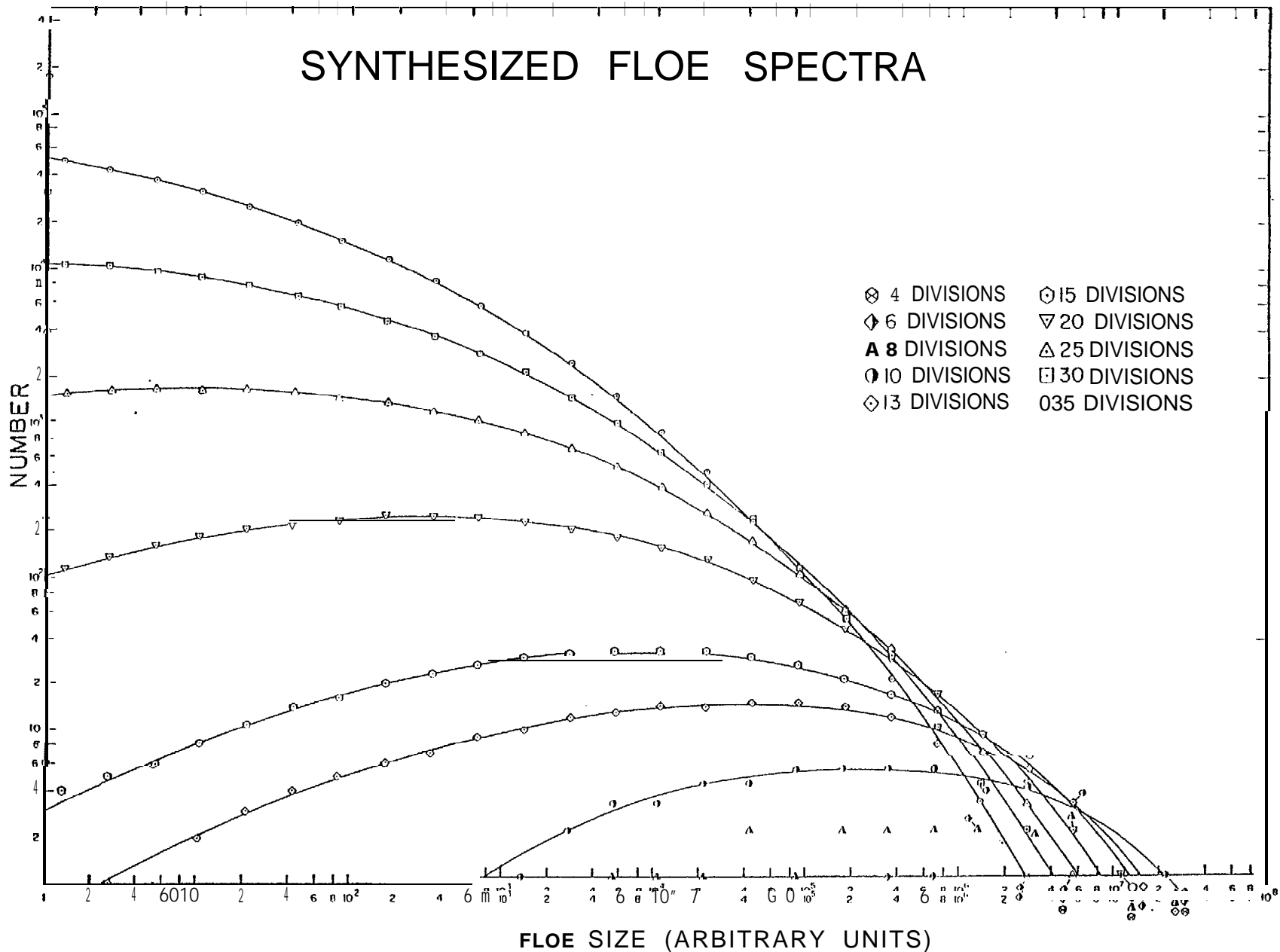


Figure 10, Synthesized distributions of floe size versus number for various numbers of floe division processes. In each case, an original floe consisting of  $10^6$  arbitrary units was divided the required number of times by a floe-splitting algorithm. The process was repeated 100 times and the results averaged. Smooth curves connect the floe size spectra thus generated. The results for few than 10 division processes were too "noisy" to be fitted with smooth curves.

## Discussion

It is perhaps best to first discuss the results of the computer simulation and then consider the measured size spectra in light of these results. Before discussing the results of the computer simulation, it must be emphasized that the algorithm used was only an estimation reflecting personal experience and what appeared to be common-sense logic. It was utilized in order to gain some insight concerning floe size distributions.

Examination of figure 10 shows that starting with the same original floe size, as more divisions are performed, the **largest** remaining floe becomes smaller. Certainly this is as would be expected. However, although very small **floes** are created in great profusion, even after 35 divisions, the largest floe is still about 3% of the area of the original floe. In other words, despite the fact that many divisions have been possible, some relatively large floes survive. As a result, one would expect that with the advance of time **large** populations of increasingly smaller floes would be created, yet some **large** floes would remain. In fact, one might anticipate a **visual** appearance of many **very** small floes with a few anomalously large floes spread throughout the pack. Late " summer Landsat imagery of nearshore ice often has this appearance. This effect is an artifact of both the floe-splitting fraction function and the portion of the algorithm determining whether division of any kind takes place.

Another feature of this family of curves is the rapid motion of the floe size distribution peak to **smaller** floe sizes with increase in number of **floe** divisions. Between the curves representing 10 and 20 divisions this peak moved over a range of  $10^4$  in floe size. However, over that same range of divisions the number of floes in the peak size categories increases by only about 1 1/2 orders of magnitude.

This observation along with the earlier observation concerning the size of the largest remaining floes can be interpreted as indicating that this algorithm creates increasingly smaller floes in considerable quantity at a rapid rate, but not in such a way to severely deplete the ranks of larger floes. At first they may seem to be a contradiction. However, only one floe size of  $10^6$  (arbitrary units) is required to produce  $10^4$  floes of size  $10^2$  units. (The algorithm is applied to an area originally comprising  $10^8$  units). Therefore, a great quantity of small floes can be created at the expense of only a few large floes comprising only a small fraction of the study area.

Having examined the consequences of a "common sense" algorithm, the discussion of the actual observed size spectra may be more meaningful. The first observation is that the measured spectra have average maximum floe sizes between  $10 \text{ km}^2$  for June and  $1 \text{ km}^2$  for August. The maximum floe sizes shown on the synthetic spectra range between  $3 \times 10^6$  units for 35 divisions and  $2 \times 10^7$  units for 15 divisions. These ranges in values are similar and would generally coincide if one unit is  $1 \text{ m}^2$ . Since the synthetic spectra were generated beginning with an area of  $10^8$  units, this would imply that for comparison purposes, the count of division processes should start when the original floe size is somewhere on the order of  $100 \text{ km}^2$ .

The next observation is that the slopes (power law exponent) of the synthetic spectra and measured spectra are similar in the regions where they can be compared, and generally became steeper with advance of season,

Unfortunately, it was not possible to measure sufficiently small floe sizes by the method used to compare size distribution peaks between the synthetic and measured spectra. Perhaps this could be done for a situation corresponding to a small number of divisions at an earlier date.

It is tempting to consider direct comparison of synthetic and measured spectra (by superposition). In order to do this, a scale factor must be considered. If the measured spectra indicate an original floe size in the vicinity of  $100 \text{ km}^2$  then the floe size distributions measured from  $100 \text{ km}^2$  areas should be generally comparable with the synthetic spectra while the floe size distributions from the  $400 \text{ km}^2$  areas should be divided by 4 for comparison purposes. Detailed comparison will yield more precise scale factors between measured and synthetic spectra. Starting with the August data, we have  $N = .7 \text{ KS}^{-1.9}$  for the  $100 \text{ km}^2$  area and  $.5 \text{ KS}^{-1.8}$  for the  $400 \text{ km}^2$  area (after application of the area factor:  $1/4$ ). Thus, these spectra are in reasonably close agreement. This might be expected since there were many small floes in the August Landsat scene so that floe statistics might be expected to be somewhat uniform. Comparison with a power-law fit to the synthetic spectra over the same size range shows that 30 divisions yield a power law of  $N = 8 \text{ KS}^{-1.5}$  while 35 divisions yield a power law of  $N = 6 \text{ KS}^{-1.7}$ . It is likely that 40 or more divisions would be required to produce a power of  $-1.9$ . Thus, it would appear that the August data correspond to somewhere between 35 and 40 floe divisions.

The July data yield area-corrected power spectra of  $N = 2.5 \text{ KS}^{-.7}$  ( $100 \text{ km}^2$ ) and  $N = 1.2 \text{ KS}^{-1}$  ( $400 \text{ km}^2$ ). Because of generally larger floe

sizes in the count areas, fewer floes were counted. Furthermore, the data were taken from different Landsat scenes. Comparison with the synthetic spectra shows that the algorithm used produces a spectrum of  $N = 17 \text{ KS}^{-0.9}$  for 15 floe divisions.

The June data yield area-corrected power spectra of  $N = 2.3 \text{ KS}^{-*6}$  ( $100 \text{ km}^2$ ) and  $N = 1.6 \text{ KS}^{-1.1}$  ( $400 \text{ km}^2$ ). The synthetic spectrum for 10 divisions is  $N = 17 \text{ KS}^{-*7}$  while for 15 divisions it is  $N = 20 \text{ KS}^{-1.1}$ . As can be seen on figure 1, the two areas chosen are separated by some distance. It is conceivable that they may have had different division histories.

In all the above examples the size coefficient of the measured spectrum is considerably lower than that of the corresponding synthetic spectrum. On the average this factor is approximately one order of magnitude. This suggests that the characteristic synthetic floe spectra correspond to a count in an area ten times as large as the area of the measured count, or  $1,000 \text{ km}^2$ .

#### Exposed Perimeter

A major item of interest from an environmental assessment point of view is the total ice floe perimeter exposed to the water. The perimeter of the surface of a regular figure is proportional to the square root of the surface area. The factor of proportionality,  $F_p$ , is usually a number somewhere in the vicinity of 4, (For a circle it is  $\pi$ , for a square it is 4, etc.) The total perimeter exposed is proportional to the sum of the square roots of the floe areas (called the characteristic floe dimension).

Assuming that the floe size spectrum algorithm produced a meaningful floe size spectrum, **the** square roots of the floe size or characteristic floe dimensions were summed for each of the average floe size spectrum calculations. The results are given below:

Original area:  $10^8$  arbitrary units

Original Characteristic floe dimension:  $10^4$  arbitrary units

Division Algorithms Performed	Summed Characteristic Floe Dimensions
10	$10.1 \times 10^4$
15	$11.4 \times 10^4$
20	<b><math>12.9 \times 10^4</math></b>
25	<b><math>13.7 \times 10^4</math></b>
30	$14.4 \times 10^4$
35	$15.8 \times 10^4$

At first this result seems strange. An area originally having a perimeter of  $10^4$  units has a perimeter only 16 times as great after undergoing the splitting algorithm 35 times. However, a simple calculation shows that this result could have been anticipated. Consider a square with perimeter  $4X$ . If this square undergoes two equal divisions (cutting it in **half** both ways), we have 4 squares with a total new perimeter of  $8X$ . Another two divisions splitting each square resulting from the first two divisions results in 16 squares with a total perimeter of  $16X$ . The result of two divisions doubles the perimeter. Four divisions quadruples the perimeter. The total perimeter is directly proportional to the **number** of divisions. However, our floe-generating algorithm only divides half the floes each time it is performed. Hence, we would expect the algorithm to increase total perimeter above the perimeter of

the original area by a factor of the number of division algorithms performed divided by two or  $P = \frac{n}{2}(F_p X)$ , where  $n$  is the number of algorithms performed,  $X$  is the characteristic dimension of the original floe and  $F_p$  is the factor of area proportionality. The results of table 1 show that this is generally the case.

On the other hand, the algorithm devised here increases the number of floes by a factor of  $(\frac{3}{2})^n$  where  $n$  is the number of times the algorithm is performed. Hence, while the total exposed floe perimeter increases linearly, the **total** number of floes increases exponentially with the number of divisions performed. This result would be generally true of any floe-splitting algorithm, although its precise expression would depend on the specific algorithm logic.

The implication of this result to environmental assessment is as follows: (1) In the case that oil is entrained within the ice and released upon melting of the ice at its perimeter, the rate at which petroleum would be released would be proportional to the total perimeter exposed at any time, or in our case roughly

$$R_1 \approx P = \frac{1}{2} n F_p X$$

(2) In the case that spilled petroleum were pooled beneath the ice and released quickly upon the formation of a new floe edge across a pool location, the number of pools exposed per unit time would determine the rate at which such releases took place. This would be proportional to the rate of change in perimeter, or in our case, roughly

$$\frac{dP}{dt} = \frac{d}{dt} \left( \frac{1}{2} n F_p X \right) = \frac{1}{2} (F_p X) \frac{dn}{dt}$$

where  $X$  (from the above explanation) is the nominal dimension of the

original floe size. Thus , the rate at which petroleum was released would be directly proportional to the rate of floe divisions taking place.

Adding  $R_1$  and  $R_2$  we have  $R$ , the total rate at which petroleum is released:

$$R = R_1 + R_2 \approx \frac{1}{2} (F_p X) \left( n + \frac{dn}{dt} \right)$$

Adding empirical factors,  $f_1$  and  $f_2$  to change these proportionalities to equations, we have:

$$R = \frac{1}{2} (F_p X) \left( f_1 n + f_2 \frac{dn}{dt} \right)$$

Assuming that  $n$  is linear in time:  $n = Nt$ , we find that the total petroleum released to be:

$$\epsilon = \int_{T=0}^{t=T} R dt = \frac{1}{2} (F_p X) \left[ f_1 \left( \frac{N}{4} T^2 + c_1 \right) + f_2 \left( \frac{NT}{2} + c_2 \right) \right]$$

where  $c_1$  and  $c_2$  represent quantities of oil introduced upon setting up the initial condition.

The value of these initial quantities can be obtained by going back to the consideration of total exposed perimeter. If one starts with an initially unbroken ice sheet, it is obvious that the total exposed perimeter changes catastrophically upon the initial breaking of the ice sheet into the sheet into the initial floes. In our computer simulation we stated with an initial floe of  $10^8$  arbitrary units<sup>2</sup> which had a perimeter proportional to  $10^4$  arbitrary units.

In our calculations X is the nominal dimension of the original floe. At the time of initial breakage, the total perimeter exposed allowing pooled oil to escape would be 4X. At T=0 the second term representing leakage of petroleum from newly exposed floe edges should be equal to  $f_2(F_p X)$ , hence  $c_2=1$ .

The other constant sets the initial condition for the term representing the constant rate of introduction of petroleum from all floe edges regardless of their age. Again at T=0 the first term should be equal to  $f_1(F_p X)$  so that  $c_1=1$  as well.

Hence:

$$\varepsilon = F_p X [f_1 \left(\frac{N}{4} T^2 + 1\right) + f_2 \left(\frac{N}{2} T + 1\right)]$$

- (1) Where  $f_1$  is an empirical number related to the release of entrained petroleum
- (2) Where  $f_2$  is an empirical number related to the release of pooled petroleum
- (3) Where X is the nominal dimension of the original floe size
- (4) Where N is the rate of floe breakages per unit time
- (5) Where T is the total time elapsed since the initial floe breakage
- (6) Where  $F_p$  is the factor of proportionality (a number in the vicinity of 4 relating floe perimeter to floe characteristic dimension)

It is likely that  $f_1$  would generally be smaller than  $f_2$  (both would have units of rate of petroleum released per unit length per unit time) and therefore, the second term (related to introduction of pooled oil) would originally be the larger of the two, but at

$$T = \frac{2 f_2}{f_1}$$

the terms would be of equal importance and the term representing introduction of entrained petroleum would dominate thereafter. Finally, the pooled petroleum term would cease to apply after the floe sizes became on the same order of magnitude as the size of the underside petroleum pools: new divisions would not expose new pools for drainage.

Some estimate must be made for N, the number of divisions per unit of time. If, as discussed earlier, the early June data correspond to between 15 and 20 floe divisions, while the early August data correspond to between 30 and 35 floe divisions, we have approximately 15 divisions taking place in 60 days or  $N = 1/4$  divisions per day.

Again, assuming  $N(t) = \text{constant}$ , this would place the original breakup of the ice into the characteristic floe sizes in early April. Observations show that the shear zone often moves into the nearshore area about this time, breaking up the fast ice seaward of the grounded ridges.

The original characteristic floe size was estimated to be in the vicinity of  $100 \text{ km}^2$  on the basis of comparison of synthetic and measured floe size spectra. The concept of an original characteristic floe size deserves some expansion. Generally in late winter and early spring, the shear zone is relatively inactive, and at times located far from the nearshore area. Then, as part of a dynamic ice event, the fast ice in the nearshore area breaks up and thereafter does not freeze together again. During this initial break up, floes of various sizes are created, starting with small floes toward the edge of the fast ice and progressing toward large floes with distance seaward. There is a tendency for the entire shear zone to break into a number of large floes immediately when this process takes place. Then the floe division process is initiated. These large floes correspond to the original characteristic floe in the algorithm.

Figure 11 shows Landsat scene E-2467-21172 showing a portion of the Beaufort Sea shear zone on May 3, 1976. Landfast ice can be seen in the lower portion of the image. A variety of floes can be seen with sizes ranging from 3200 km<sup>2</sup> to a few square km. A number of floes with areas in the vicinity of 50 to 150 km<sup>2</sup> can be seen. In addition, several floes can be seen undergoing division, including the 3200 km<sup>2</sup> floe (see arrows.) Clearly, the floe division process has been underway for some time and a number of small floes have been generated. In addition, a very large floe remains from the initial breakup process. It, in turn, is in the process of calving a floe with an area in the vicinity of 200 km<sup>2</sup>.

This image shows that while the concept of an original floe size in the vicinity of 100 km<sup>2</sup> has some merit, it would probably be more realistic to begin the floe-generating algorithm with some initial floe size distribution resulting from the initial breakup of the shear zone ice.

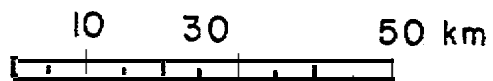
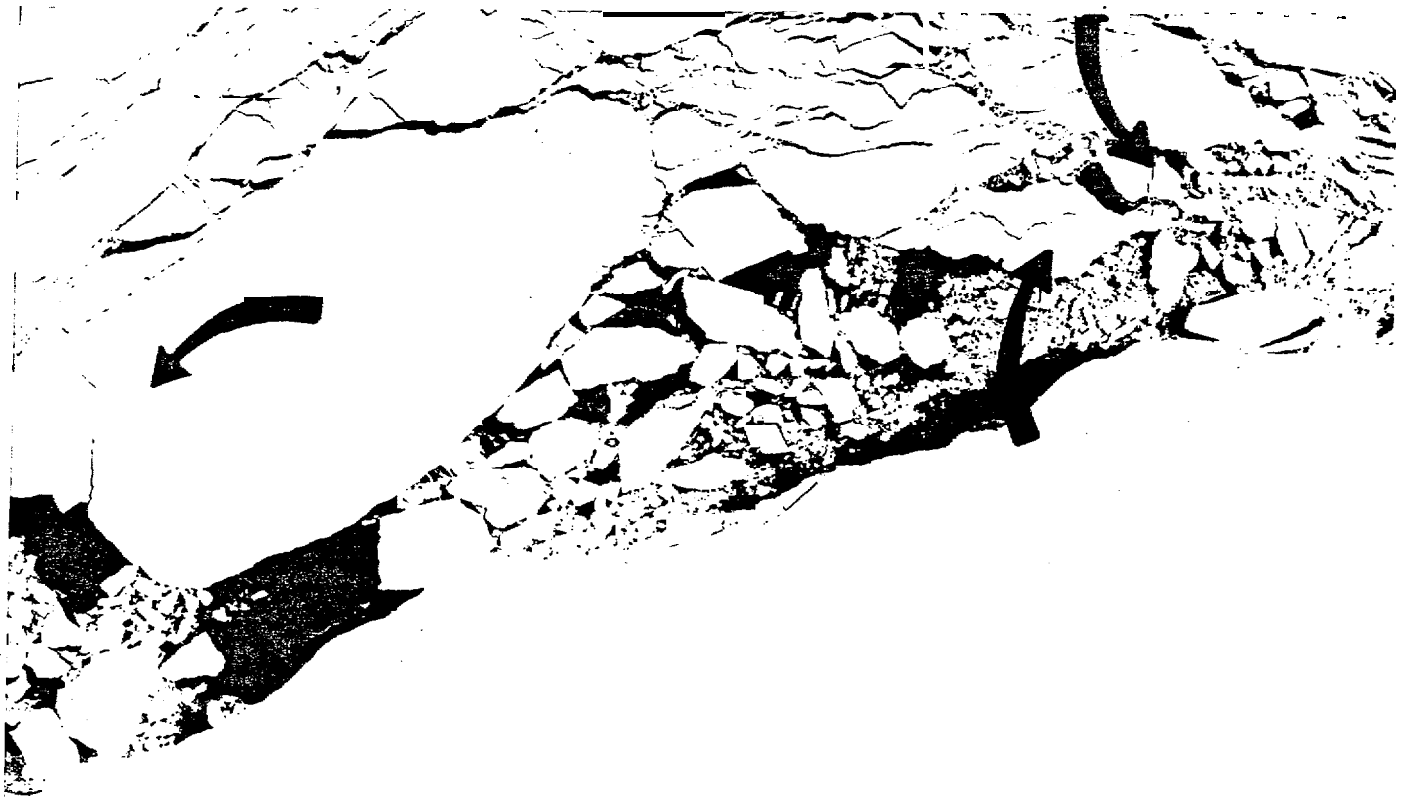


Figure 11. Landsat scene E-2467-21172 showing a portion of the active Beaufort Sea shear zone on May 3, 1976. Landfast ice covers much of the lower portion of the image. This image was chosen to show typical floe sizes at this early stage of the floe-division process. Arrows point to floes undergoing division at this time.

## Conclusions

- (1) Measured nearshore floe size spectra obtained between June and August exhibit a power law distribution  $N = N_0 K S^{-\alpha}$  over the range  $0.03 < S < 40 \text{ km}^2$ . The observed value of  $\alpha$  varies generally systematically with time from a low value of 0.6 in June to 1.9 in August.
- (2) Synthetic floe size spectra were generated by means of a simple division algorithm which divides every other floe at each iteration. Floes are divided by means of the ratio obtained by randomly selecting a number between 1 and 100. This distribution is broadly peaked about a .5 division. These synthetic spectra exhibited a wide range of floe sizes even after a few iterations of the algorithm. Although these spectra were clearly not power law distributions, it was only possible to compare these spectra with the measured spectra over a short range of the synthetic spectra. Over this short range, the synthetic spectra could be approximated with a lower law distribution. Comparison of the measured spectra with this portion of the synthetic spectra showed agreement assuming that by June between 10 and 15 floe divisions according to our proposed algorithm had taken place, by July 15 divisions had taken place and by August 35 divisions had taken place. Assuming a constant rate of floe division (half the floes divide every four days), this rate of floe divisions projects an initial floe formation to take place around April.
- (3) Comparison of the synthetic and measured spectra further suggest that an original characteristic floe size of area approximately  $100 \text{ km}^2$  occurs upon the breakup of the nearshore ice.

(4) Perimeter tabulations show that although the total number of floes increases exponentially, the **total** floe perimeter increases only by a factor of approximately  $\frac{n}{2}$  times the characteristic original **floe** perimeter (where n is the number of floe division algorithms which have been applied,)

(5) The implications of the perimeter results have been examined in terms of two sources of introduction of petroleum into the sea:

(1) a new floe edge forming across an under-ice pool

and

(2) Melting of ice surrounding entrained ice at the edge of floes.

The first process was found **to** be proportional to the rate at which new floes are forming,  $\frac{dn}{dt}$ , while the second was found to be **directly** proportional **to** n. Consideration of the integrals of these functions suggests that in general **the** first process **will** be most important at first, but **will later** give way to the second. **The** time at which this takes **place** is dependent upon the ratio of two empirical constants relating **the** availability of pooled oil to lead formation, and the concentration of petroleum entrained within the sea ice.

## References

- Crowder, W.K., H.L. McKim, S.F. Ackley, W.D. Hibler, III, and D.M. Anderson  
"Mesoscale deformation of sea ice from satellite imagery," Interdisciplinary  
Symposium on Advanced Concepts and Techniques in the Study of Snow  
and Ice Resources, 1973.
- Kovacs, A., and M. Mellor, "Sea Ice morphology and ice as a geologic agent  
in the southern Beaufort Sea, The Coast and Shelf of The Beaufort Sea,  
Reed, J.C. and J.E. Sater, eds, 1974.
- Stringer, W.J. "Morphology of the Beaufort Sea shorefast ice, The Coast  
and Shelf of the Beaufort Sea, Reed, J.C. and J.E. Sater, eds, 1974.

## Acknowledgements

This study was funded wholly **by the** Bureau of Land Management through interagency agreement with the National Oceanic and Atmospheric Administration, as part of the Outer Continental Shelf Environmental Assessment program.